A MODIFIED METHOD-OF-MOMENTS TECHNIQUE FOR THE FULL-WAVE ANALYSIS OF IMPERFECT CONDUCTORS ON LOSSY AND FINITE-EXTENT SUBSTRATES

Martin Gimersky and Jens Bornemann

Laboratory for Lightwave Electronics, Microwaves and Communications (LLiMiC)
Department of Electrical and Computer Engineering
University of Victoria, Victoria B.C. Canada V8W 3P6

ABSTRACT

A modified method-of-moments technique with general field-solver capability is presented. The structure to be analyzed is subdivided into a number of thin-wall cells. Surface impedance concepts are used to represent the material characteristics of each cell. The outstanding advantages of this method include: the absence of absorbing boundary conditions, as material parameters are defined with respect to a surrounding environment, e.g., free-space, thus minimizing the computational domain; conductor and dielectric losses are readily incorporated via the surface impedance concept; and radiation into any direction, even below the ground-plane of a finite-extent substrate, is included.

Several examples involving imperfect conductors as well as lossy and finite-extent dielectric substrates are presented. The method is compared with measured results and is found to be in good agreement.

I. INTRODUCTION

Frequency-domain numerical techniques are well known for their ability to solve complex structures in passive microwave structures, e.g. [1]. They are, to various degrees, capable of including conductor, dielectric and radiation losses. The cross-sectional structure complexity has recently been increased by applying established time-domain techniques in the frequency domain, e.g. [2] - [4]. All of these methods require, however, defined boundaries for the computational space. These can either be specified as electric/magnetic walls [2], [3], or as absorbing boundaries [4] - [6], which gave rise to a new research area in electromagnetic field modelling.

The method of moments, e.g., [7], is predominantly used for radiation analysis and distinguishes itself from many other techniques by the noticeable absence of absorbing boundaries. However, microwave printed circuit analysis, such as common in (M)MIC design, is usually not among the standard applications for the method of moments.

Therefore, this paper focuses on a modified method-of-moments technique, which not only incorporates the losses of conductors and dielectrics, but also the effects of finite-extent circuits and substrates in free-space environment. Several examples demonstrate that this technique is capable of solving general electromagnetic problems.

II. THEORY

The modified-method-of-moments technique is largely based on earlier work by Rubin and Daijavad [8]. However, we replaced the somewhat arbitrary numerical integration process with a solid and 'tuning-free' algorithm and implemented suggestions in [8] on conductor and substrate losses, which are considered a prerequisite for any meaningful integrated circuit analysis nowadays. The fundamental steps are outlined below and include some modification compared to [8].

Fig. 1 demonstrates the subdivision of a planar microwave structure into thin-wall sections. Each such cell is represented by half-rooftop current functions. For a single cell (N_x=N_y=N_z=1), the number of currents required is 12, but in practical applications, the average number of currents per cell, P_{av}, is reduced by the connection to neighbor cells (Fig. 2) and can be written as

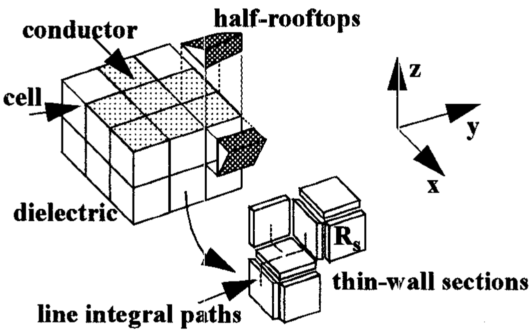

Figure 1: *Subdivision of a planar microwave structure into thin-wall sections.*

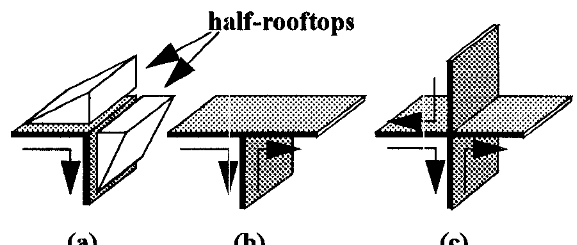

Figure 3: *Representation of junction currents. (a) At an external edge; (b) at a three-junction; (c) at a four junction.*

0-7803-3246-6/96/$5.00 © IEEE

$$P_{av} = 9+2\left(\frac{1}{N_x}+\frac{1}{N_y}+\frac{1}{N_z}\right)-\left(\frac{1}{N_xN_y}+\frac{1}{N_xN_z}+\frac{1}{N_yN_z}\right) \quad (1)$$

Although this number is larger than that of, e.g., a finite-difference analysis, note that the computational space is smaller, as we need not model the surrounding environment.

Material properties are incorporated through the cell's total impedances, e.g. R_x in x-direction. For the thin-wall structure, however, the surface impedance must be such that when multiplied by length τ_x and divided by perimiter $2(\tau_y + \tau_z)$, the result is again R_x. Thus, the surface impedance along x, R_{sx} [Ω] (Fig. 3), is given by

$$R_{sx} = 2\left[\frac{1}{\tau_y}+\frac{1}{\tau_z}\right] / [j\omega\varepsilon_0(\varepsilon_r - 1)] \quad (2)$$

where expressions

$$\varepsilon = \varepsilon' - j\varepsilon'' = \varepsilon_0\varepsilon_r - j\sigma/\omega$$

$$R_{sx,y,z} = (1+j)/(\delta\sigma) \quad (3)$$

are used for imperfect dielectrics and conductors, respectively. Note that the permittivity in (2), utilizing the volume equivalence theorem [12], is defined with respect to the surrounding free-space environment.

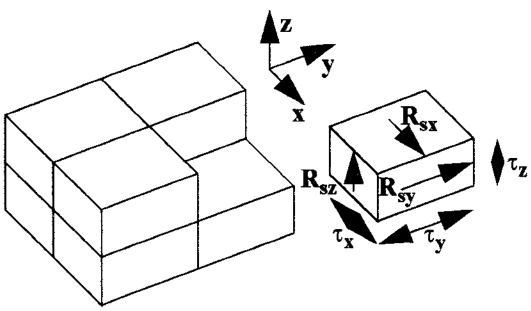

Figure 3: *Surface impedances on individual cells.*

The electric field boundary condition, applied over each dielectric cell wall and conductor surface, is

$$\mathbf{E}_t^{scat} - \mathbf{J}_s R_s = -\mathbf{E}_t^{inc} \quad (4)$$

where the incident field is related to the applied voltage by

$$V_\beta = -\int_{u_{1\beta}}^{u_{2\beta}} \mathbf{E}^{inc}(x,y,z)\cdot\mathbf{e}_{u\beta}du \quad (5)$$

Since the scattered field can be written as $\mathbf{E}^{scat} = -j\omega\mathbf{A} - \nabla\Phi$, the entries of the impedance matrix $Z_{\beta\alpha}$ are obtained as

$$Z_{\beta\alpha} = -\int_{u_{1\beta}}^{u_{2\beta}} \left[\frac{1}{4\pi}\sum_{\alpha=1}^{P}\left(j\omega\mu_0 F_A \mathbf{e}_{u\alpha} + \frac{1}{j\omega\varepsilon_0}\nabla\left(F_S^f - F_S^r\right)\right) + \frac{\tau_{v\alpha}}{2(\tau_{v\alpha}+\tau_{w\alpha})}R_{s\alpha}R'_\alpha(x,y,z)\,\mathbf{e}_{u\alpha}\right]\mathbf{e}_{u\beta}du \quad (6)$$

In (5) and (6),

$$R'_\alpha(x,y,z) = \begin{cases} q_{\tau_{u\alpha}}(u-u_\alpha)\,p_{t_{v\alpha}}(v-v_\alpha) & w = w_\alpha \\ 0 & w \neq w_\alpha \end{cases} \quad (7)$$

are the rooftop functions, $\mathbf{e}_{u,v,w}$ are the unit vectors in the directions of current flow (see [8] for details), and integrals $F_{A,S}$ are given by

$$F_A = \iint q_{\tau_{u\alpha}}(u'-u_\alpha)\,p_{\tau_{v\alpha}}(v'-v_\alpha)\frac{e^{-jkr(u-u',v-v',w-w_\alpha)}}{r(u-u',v-v',w-w_\alpha)}du'dv' \quad (8)$$

$$F_S^{f/r} = \frac{1}{\tau_{u\alpha}}\iint p_{\tau_{u\alpha}}\left(u'-u_\alpha \mp \frac{\tau_{u\alpha}}{2}\right)p_{\tau_{v\alpha}}(v'-v_\alpha)\frac{e^{-jkr(u-u',v-v',w-w_\alpha)}}{r(u-u',v-v',w-w_\alpha)}du'dv' \quad (9)$$

where f/r denotes the falling/rising half-rooftop.

In order to evaluate (8) and (9), a transformation to the polar coordinate system is performed [9]. This eliminates the singularities in the general two-dimensional exponential intergals, and a stable solution, free of any 'numerical tuning', is obtained. For details on this procedure, the reader is referred to [9].

For a given voltage excitation vector, the current distribution, from which circuit responses and radiation characteristics are calculated, is obtained by inverting the impedance matrix. Since the integration procedure is stable, the entries of the impedance matrix are well defined, and so are the individual currents.

III. RESULTS

Fig. 4 shows a comparison between this method and values from [10] at the example of the input reflection coefficient of an offset-fed microstrip radiator. Good agreement is obtained over the entire frequency range with the only exception of the resonance at 10.18 GHz. This resonance was found to depend on the length of the feeding line, as discussed in [10], whereas the other three resonances remain uninfluenced by this effect and, therefore, are clearly attributed to the radiator. In our calculation, the feeding line length (not specified in [10]) was long enough to move this resonance below 4 GHz.

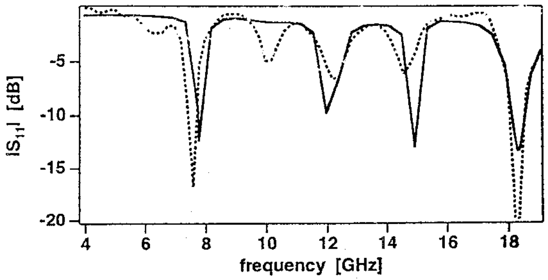

Figure 4: *Input reflection coefficient of the asymmetrically edge-fed patch according to [10]. Solid line: this method; dashed line: measurements [10].*

A shorted microstrip line wrapped around three sides of a bottom-metallized dielectric cube is depicted in Fig. 5 (top). A delta gap is retained for feeding purposes. The complex input impedance is shown at the bottom of Fig. 5. In comparison with the input reactance calculated in [8], we obtain agreement only in principle. First, while our integration procedure is stable, the questionable algorithm proposed in [8] is unstable to a degree where the entire curve can be moved and positioned at any frequency of Fig. 5.

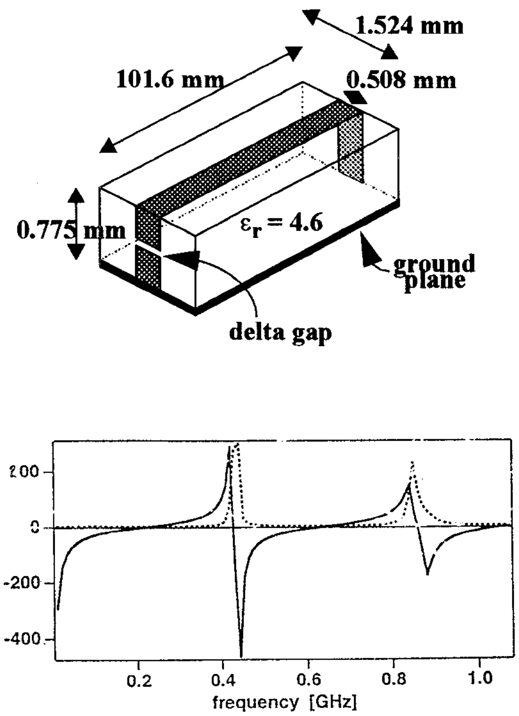

Figure 5: *Input impedance of a delta-gap fed shorted microstrip line. Solid line: imaginary part; dashed line: real part.*

Secondly, at very low frequencies, our input impedance correctly approaches $-j\infty$ [11], whereas the one in [8] does not. Thirdly, the next resonance, which must appear at around twice the frequency of that of the fundamental one - as shown in Fig. 5 - is not produced by the method of [8].

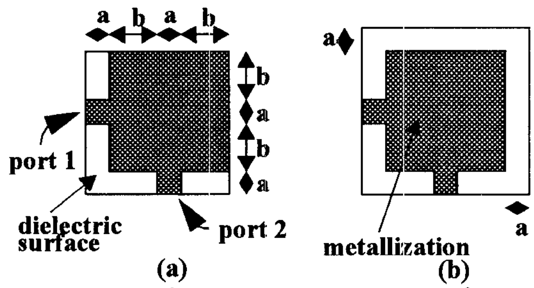

Figure 6: *Rectangular microstrip resonator on finite-extent substrates. Dimensions: a=1.036 mm, b=2a; dielectric thickness 1.423 mm; material properties are those of gallium arsenide at 25°C.*

The influence of the finite-extent substrate is investigated at the example of Fig. 6. The material properties selected are those of GaAs. Due to the relatively high permittivity, the performances of the circuit of Fig. 6a (dashed lines in Figs.7) and that of Fig. 6b (solid lines in Figs.7) differ only slightly. The structure of Fig. 6a certainly has higher fringing fields - note that the extent of the ground metallization varies with the substrate size - and, therefore, resonances are observed at lower frequencies (Figs. 7a, b).

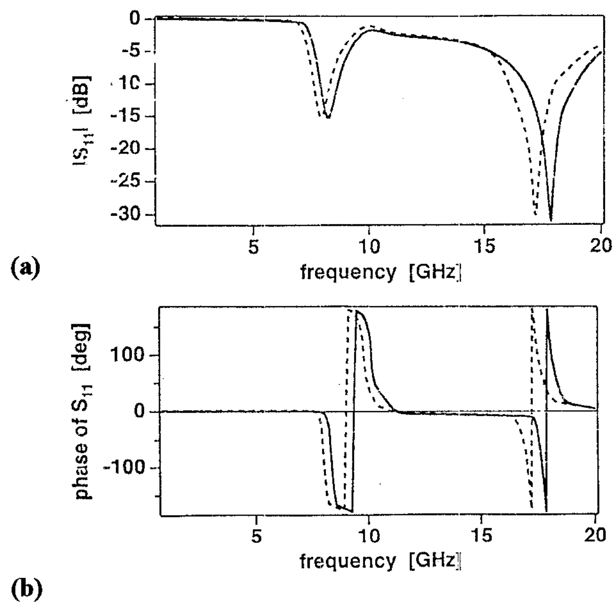

Figure 7: *Performance of rectangular microstrip resonator. a) input reflection; b) input reflection phase.*

Figs. 7c, d show the transmission response. Although magnitude and phase of S_{21} comply with expectations, in the sense that the largest phase variation is observed at resonance, an agreement with the input reflection performance of Figs. 7a, b is difficult to envision at first sight. However, if we look at the radiation versus frequency in Fig. 7e, what seems to be a contradiction, is easily resolved. At the two S_{11} resonances (Fig. 7a), most of the input power is radiated by the microstrip resonator (Fig. 7e). In between these two frequencies, radiation is significantly reduced and a substantial amount of power reaches the second port, thus causing a maximum in the transmission coefficient S_{21} (Fig. 7c). This example demonstrates the capability of the modified method-of-moments technique to predict complicated relationships in modern microwave integrated circuits.

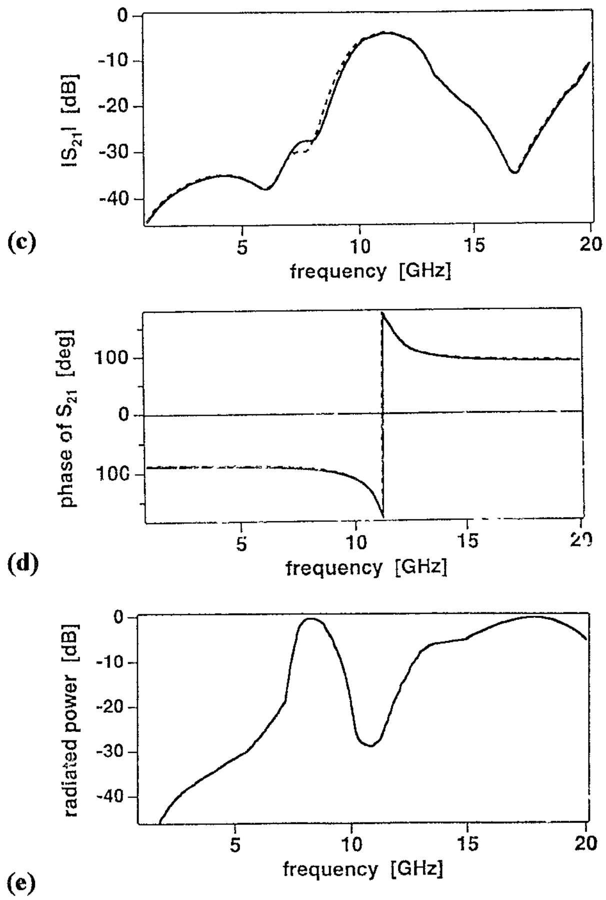

Figure 7 (cont'd): *Performance of rectangular microstrip resonator. c) transmission; d) transmission phase; e) radiation.*

IV. CONCLUSIONS

A modified method-of-moments technique for the analysis of (monolithic) microwave integrated circuits is presented. The method is based on a subdivision of the structure into thin-wall cells, whose surface impedances represent their material properties. Dielectric and conductor losses are readily incorporated. Although effects due to radiation are fully included, the surrounding environment need not be modelled, as material parameters are defined in relation to a homogeneous medium, e.g., free space. The method is demonstrated at three examples. Good agreement is obtained with measured results.

REFERENCES

[1] R. Sorrentino, *Numerical Methods for Passive Microwave and Millimeter Wave Structures.* New York, NY: IEEE Press, 1989.

[2] H. Jin and R. Vahldieck, "Full-Wave Analysis of Guiding Structures Using a 2-D Array of 3-D TLM Nodes", *IEEE Trans. Microwave Theory Techn.*, Vol. 41, pp. 472-477, Mar. 1993.

[3] S. Xiao, R. Vahldieck and H. Jin, "A fast two dimensional FDTD full-wave analyser with adaptive mesh size", in *1992 MTT-S Int. Microwave. Symp. Dig.*, pp. 783-786, 1992.

[4] V.J. Brankovic, D.V. Krupezevic, and F. Arndt, "An efficient two-dimensional graded mesh finite-difference time-domain algorithm for shielded or open waveguide structures", *IEEE Trans. Microwave Theory Tech.*, Vol. 40, pp. 2272-2277, Dec. 1992.

[5] V.N. Kanellopoulos and J.P. Webb, "A numerical study of vector absorbing boundary conditions for the finite-element solution of Maxwell's equations", *IEEE Microwave Guided Wave Lett.*, Vol. 1, pp. 325-327, Nov. 1991.

[6] D.S. Katz, E.T. Thiele and A. Taflove, "Validation and extension to three dimensions of Berenger PML absorbing boundary condition for FD-TD meshes", *IEEE Microwave Guided Wave Lett.*, Vol. 4, pp. 268-270, Aug. 1994.

[7] R.F. Harrington, *Field Computation by Moment Method.* Malabar, FL: Krieger Publishing Co., 1987.

[8] B.J. Rubin and S. Daijavad, "Radiation and scattering from structures involving finite-size dielectric regions," *IEEE Trans. Antennas Propagat.*, vol. 38, pp. 1863-1873, Nov. 1990.

[9] M. Gimersky, S. Amari and J. Bornemann, "Tuning-free analysis of planar radiators based on an exact numerical evaluation of the two-dimensional generalized exponential integral", in *1995 IEEE-APS Int. Symp. Dig.*, pp. 1316-1319.

[10] S.-C. Wu, N.G. Alexopoulos, and O. Fordham, "Feeding structure contribution to radiation by patch antennas with rectangular boundaries", *IEEE Trans. Antennas Propagat.*, Vol. 40, pp. 1245-1249, Oct. 1992.

[11] A.S. Schelkunoff, *Electromagnetic Waves.* Princeton, NJ: Van Nostrand, 1964, ch. 12.

[12] C.A. Balanis, *Advanced Engineering Electromagnetics.* New York, NY: John Wiley & Sons, 1989, ch. 7.